

The Dependence of Ammonal Detonation Performance on Cylinder Test Scale

Eric K. Anderson*, Scott I. Jackson

Shock and Detonation Physics Group, M-9, LANL, Los Alamos, NM, 87545, USA

Abstract

For a detonation to propagate steadily, the lead shock must be supported by energy release from the chemical reaction zone. Flow divergence cools the flow behind the compression shock, slowing chemical reactions and reducing the available energy to drive the detonation forward. This results in the diameter effect and eventually detonation failure as charge size is reduced. Similarly, the energy available to perform work on adjacent materials in the product flow tends to decrease with charge size. The performance of non-ideal explosives such as ammonium nitrate blended with aluminum powder (Ammonal) are particularly sensitive to flow divergence. In this study, the effect of flow divergence on Ammonal performance is investigated through application of an analytic method to analyze cylinder expansion (CYLEX) test wall velocity profiles for tests with inner diameters of 12.7 mm up to 76.2 mm. For these tests, the detonation velocity and detonation product isentropes and heat of detonation are reported. In addition, analysis of the velocity profiles is shown to reveal an experimental measurement of the Rayleigh line, which agrees well with the theoretical Rayleigh line for all experiments. Reaction

*Corresponding author

Email address: eanderson@lanl.gov (Eric K. Anderson)

zone times are inferred using this feature.

Keywords: detonation, non-ideal, explosive

1. Introduction

In the detonation process, the lead shock adiabatically compresses reactants to overcome their activation energy, resulting in reactions which convert the reactant to products with lower chemical potential energy. But for steady detonation propagation, this lead shock must also be supported by some of the energy released by these reactions. In this sense, detonation is a coupled fluid-chemical process.

In the case of condensed phase explosives, pressures in the reaction zone exceed the yield strength of confining materials. This results in lateral expansion of the reacting flow, which in turn decreases the temperature and pressure of that flow. The reduced temperature and pressure in the expanding reaction zone can slow or freeze reactions, leaving the detonation product in a partially reacted state. This effect reduces detonation velocity, D_0 , reaction zone length, and product energy, e_0 – the energy released by the detonation, normalized by the reactant mass. Lateral flow expansion occurs on the charge surface area, while the volumetric energy release scales with the cross sectional area of the charge. Thus, the effects of flow expansion become increasingly significant with decreasing charge size, as the surface area grows large relative to the charge volume.

These effects are especially pronounced for non-ideal explosives, where the reactions are slow relative to ideal explosives, and significantly affected by confinement effects and charge size [1, 2]. This can be seen in Fig. 1, where the scale dependence of several explosives are shown. In this figure, the detonation velocity is plotted as a function of inverse charge radius, $1/R$. The non-ideal explosives

Ammonium Nitrate and Fuel Oil (ANFO) and Ammonal display a strong dependence of D_0 on R , with steady detonation propagation in small charges observed at velocities nearly half that of the theoretical Chapman-Jouguet (CJ) velocity. PBX 9501, on the other hand, is a good example of an ideal explosive, with little change in detonation velocity as function of radius from the CJ condition to the failure diameter.

Ammonium-nitrate (AN) based explosives are commonly used in industry, particularly in the mining sector [3]. Pure AN is generally considered an oxidizer, but it can detonate on its own, displaying a large failure diameter and low detonation velocities. Blending AN with other materials to improve the oxygen balance can enhance the performance. Examples of such materials include other explosives such as TNT, combustible organic materials such as diesel fuel, and, in the case of Ammonal, a combustible metal. AN-based explosives including Ammonal are also of interest due to their availability and simple preparation.

In this work, we investigate non-ideal effects in Ammonal detonation through application of a recently refined two-dimensional (2D) analytic method [2, 4] to analyze previously reported [5, 6, 7] scaled Ammonal CYLEX tests. In a CYLEX test, an explosive is placed inside an annealed copper tube, detonation is initiated at one end, and the detonation velocity and confiner motion are measured. Analysis of the measurements can yield the pressure, P and specific volume, v of the explosive in the expanding flow behind the detonation. Integration of the isentrope in P - v space yields e_0 . For Ammonal, the analysis also yields an experimental measurement of the Rayleigh line and can be used to estimate reaction zone length at the inner surface of the confiner.

2. Experiments

The results reported were obtained using scaled CYLEX tests. The standard CYLEX test consists of a 304.8 mm (12 in.) long by 25.4 mm (1 in.) diameter explosive charge surrounded by an annealed, C101 copper confiner with nominal dimensions of 25.4 mm (1 in.) inner diameter (ID), 30.48 mm (1.2 in.) outer diameter (OD), and 304.8 mm (12 in.) length. For scaled tests, the diameter of the explosive charge is varied while the proportionality to the other dimensions is maintained. Figure 2 shows a 76.2 mm (3 in.) ID Ammonal cylinder test.

The CYLEX tests reported here utilized PDV to measure confiner wall-velocity profiles. Detonation velocity for each test was measured using time of arrival wires on the outside surface of the confiner. For each experiment, eleven wires were placed in a line, with the first wire positioned an axial distance of two charge diameters from the initiation plane. The remainder of the wires were spaced evenly between the first wire and the end of the confiner. The wires were held at 70 V and functioned by shorting to the confiner wall upon arrival of the shock wave. An oscilloscope monitoring the confiner electrical potential recorded a voltage spike each time a wire shorted. For the 50.8 mm and 76.2 mm ID tests, the detonation front shape was also measured using a Cordin 132 streak camera to image a mirror surface on the inside of a PMMA window at the end of the charge. The mirror was vapor-deposited aluminum and was in contact with the explosive. The specifics of the experiments considered in this study are detailed in Table 1.

All tests reported in Table 1 were conducted using the same 90% AN and 10% Aluminum (Al) mass fraction blend of Ammonal. This ratio results in a positive oxygen balance. Ammonal mixtures are stoichiometric with a mass ratio of approximately 80% AN and 20% Al [8]. The AN and Al particles sizes varied

between the tests. For 8-1854 and 8-1855, the Al powder had a 50% mass fraction diameter of $2.05\ \mu\text{m}$ while the AN particles were ground to a 50% mass fraction diameter of approximately $850\ \mu\text{m}$. For the LLNL tests, the AN particle diameter was $60\ \mu\text{m}$ and the Al particle diameter varied according to the table.

Tests 8-1854 and 8-1855 were prepared using pre-blended Ammonal, which was loaded into the confiner tubes gradually while the tubes were tapped by hand to prevent the formation of large air pockets. The material was weighed during the loading process and the densities shown in Table 1 were calculated from the Ammonal mass and tube inner volume. The final explosive density for these tests varied slightly as a result of the loading technique. Each test was initiated with a PETN-based detasheet booster and an RP-1 detonator. Additional experimental details on tests 8-1854 and 8-1855 are available in [6, 7].

3. Confiner Wall Velocity Profiles

The PDV technique produces an interference pattern as the outgoing laser light is mixed with Doppler shifted light returning from a moving surface [9]. This interference pattern may be analyzed to extract velocity as a function of time. The resulting velocity profiles from tests 8-1854 and 8-1855 are shown in Fig. 3. These profiles are typical of CYLEX tests for non-ideal explosives where the pressures generated are not sufficient to produce ringing associated with compressible confiner motion. Non-ideal effects are apparent in the figure, with 8-1855 (76.2 mm ID) showing lower velocities than 8-1854 (50.8 mm ID) for measurement locations near the start of the test, and higher velocities than 8-1854 for measurement locations near the downstream (or “breakout”) end of the cylinder. Thus, it appears that Ammonal reacts more completely at the larger scale, resulting in the

higher wall velocities, but it takes a significant portion of the run distance for this to develop. This is consistent with prior work, which has shown that higher D_0 values associated with larger tests yield increased energy output [10]. While steady behavior in wall velocity profiles appears to develop between 37 % and 51 %, measured detonation velocity was steady by the first shorting wire for each experiment. This suggests that energy release upstream of the sonic locus becomes steady more quickly than energy release downstream of the sonic locus.

3.1. LLNL CYLEX Data

LLNL wall velocity profiles were measured using either the PDV or Fabry techniques described in [11] for the tests summarized in [5]. Other than a correction for the 7° probe angle, the LLNL tests were analyzed using the same routine applied to tests 8-1854 and 8-1855.

3.2. Analysis of Velocity Profiles

Further processing of the PDV velocity profiles can be applied to extract product isentropes. The analysis begins with a velocity profile similar to the experimental profile shown in Fig. 4. Typically, the analytic method of computing a product isentrope from a CYLEX velocity profile begins by fitting the following equation to the data:

$$v_0(t) = \frac{v_\infty((t+1)^\alpha - 1)}{\frac{2v_\infty\alpha}{a_0}(t+1)^\alpha - 1}, \quad (1)$$

where t is time relative to first motion of the confiner at the measurement location and v_0 is the cylinder wall velocity component normal to the direction of detonation propagation [12]. The parameter v_∞ represents the asymptotic wall velocity,

a_0 is the initial acceleration value at $t = 0$, and α is a non-dimensional parameter that controls how quickly the curve approaches v_∞ . This form facilitates the analysis of cylinder test data, and rejects noise that may be present in the velocity profile. A fit to this form is shown in Fig. 4 along with a low-pass filtered velocity profile.

The fitting form of Eq. 1 does not, however, capture the confiner precursor motion accurately, as discussed in [2]. This is apparent in the inset of Fig. 4, where the same profiles are shown zoomed in on the first $5 \mu\text{s}$ of confiner acceleration. Here, the low-pass filtered velocity profile captures the confiner motion much more closely up to $1.5 \mu\text{s}$ in the figure. The remainder of the analysis described here was conducted using both the filtered and fitted velocity profiles.

Since ringing is not observable in these experiments, the 2-D method for analyzing cylinder tests with incompressible case material described by Jackson was applied [4]. With this method, the product isentrope is expressed in the pressure-specific volume plane, with pressure computed as

$$P = \frac{\rho_w}{2} \frac{(R_0^2 - R_i^2)}{r_i \cos \theta_i} \frac{dv_0}{dt}, \quad (2)$$

where ρ_w is the confiner density, and R_0 and R_i are the initial outer and inner radii, respectively. The quantities r_i and θ_i are the inner radius and wall angle, and vary with time during the expansion. Expressions for these two terms are developed in [2, 4]. The term $\frac{dv_0}{dt}$ is the wall acceleration in the direction normal to detonation propagation.

The specific volume is computed using the equation

$$v = r_i^2 A \frac{\rho_e D_0^2 R_i^2 - P r_i^2 + F_b + P_e R_i^2}{\rho_e^2 D_0^2 R_i^4}, \quad (3)$$

where ρ_e is the initial density of the explosive, P is the time-varying pressure inside the tube, and P_e is the constant pressure outside the tube. The term F_b is the axial force on the tube due to the pressure inside the tube, while A is the time-varying product-flow geometry-coefficient. Derivations for Eqs. 2 and 4 are provided in [4] with a correction in [2].

4. Product Isentropes

Isentropes computed using both a low-pass filtered velocity profile and a profile fitted to Eq. 1 are shown in Fig. 5 for the 76.2 mm ID test. In addition, the theoretical Rayleigh line is shown. This line intersects the horizontal axis at the specific volume of the unreacted explosive, and has a slope equal to $(\rho_e D_0)^2$.

Following the explosive in P - v space during detonation and expansion, the explosive starts initially on the horizontal axis at $v = v_0$. It is then compressed along the Rayleigh line, following this line up and to the left in the figure, before expanding isentropically to low pressure and high specific volume. The isentrope computed using the filtered velocity profile (green) follows the theoretical Rayleigh line closely until peak pressure in the test is reached. As the explosive product expands, however, the isentrope begins to diverge from the Rayleigh line. Also, oscillations are observed resulting from noise which the filtering process does not reject. The isentrope generated using the fitted velocity profile (blue), on the other hand, does not capture the compression along the Rayleigh line, but does produce a smooth expansion without oscillations. As in [2], composite isentropes were constructed to combine the benefits of both techniques, with the filtered pro-

file used until reaching 0.5 % divergence between the experimental Rayleigh line and the filtered isentrope. Beyond that, the fitted profile was used.

Resulting composite isentropes for Ammonal CYLEX tests ranging from 12.7 mm ID up to 76.2 mm ID are shown in Fig. 6. Large increases in maximum pressures with test ID are evident for each diameter tested. The higher pressures persist for a significant portion of the isentropic expansion, especially for $v/v_0 < 1.0$. This non-ideal behavior is in contrast with ideal explosives, where isentropes computed from CYLEX tests are consistent across scales, as long as the test scale does not approach the failure diameter for the explosive.

Fitting parameters for the JWL equation-of-state (EOS) [13] were determined for each PDV probe using the method of least squares to determine the best fit to the composite isentropes. Separate parameters are shown for each probe for tests 8-1854 and 8-1855. For comparison across scaled tests, axial probe positions are provided as percentage of run distance, where 0 % is the initiation plane and 100 % is the end of the test. JWL fitting parameters are listed in Table 2, where the parameters A , B , C , R_1 , R_2 , and ω correspond to the form

$$P = A \exp\left(-R_1 \frac{v}{v_0}\right) + B \exp\left(-R_2 \frac{v}{v_0}\right) + C \left(\frac{v}{v_0}\right)^{-(1+\omega)}. \quad (4)$$

In Fig. 7, isentropes are shown for 68% run distance for tests 8-1854 and 8-1855. The black circles represent points along the isentrope directly computed from the measured velocity profiles. The Rayleigh line for each test is shown in pink, with the computed CJ point marked by a solid pink circle. The red curve shows the JWL fit to the experimental data, with the parameters reported in Table 2.

Recently, an empirical correlation model relating the product energy, e_0 , to

the kinetic energy of reactants in the shock frame, $S = \rho_0 D_0^2$ was described in detail in [10]. Additionally, the model provides a method to predict the product pressure as a function of specific volume. The resulting curves are plotted as the blue lines in Fig. 7. While the JWL fits to the experimental isentropes show better qualitative agreement, the model shows remarkably good agreement considering that the only inputs to the model are the experimentally measured initial density, ρ_0 , and phase velocity, D_0 .

5. Detonation Product Information

The JWL fits of Table 2 can be used to calculate the specific JWL energy, e_0 , of detonation products. To compute e_0 , the area under the isentrope represented by the JWL is integrated. The integration limits were set to include the area beginning at isentrope intersection with the Rayleigh line out to a product specific volume of 7 times the reactant specific volume.

Energies calculated by this method are plotted in Fig. 8. In the figure, e_0 is plotted as a function of reactant kinetic energy in the shock frame. Across the range of cylinder test sizes reported, product energy and reactant kinetic energy increase with test scale. This suggests that for these test scales, the energy released both before and after the detonation sonic surface is strongly scale-dependent. Similar results were observed for ANFO in [2]. It should be noted that the values shown in this figure were computed for tests with varying Al particle diameter. While the effect of particle diameter has not been well characterized for Ammonal, other explosives have shown a weak inverse correlation between particle size and measured detonation velocity, and particle size and product energy [14, 15].

Reaction times at the inner wall of CYLEX tests can be estimated by taking

the difference between the velocity jump-off time to the time where the isentrope diverges 0.5% from the Rayleigh line. Using this technique, reaction times were computed and are plotted on the vertical axis of the plot in Fig. 9. These times are plotted against estimated acoustic transit time across the confiner wall, computed as twice the confiner wall thickness divided by the confiner sound speed. The acoustic transit time provides an estimate of the time high pressure is maintained at the inner surface of the confiner, with corresponding high temperatures allowing reactions to continue.

While there is a fair amount scatter, the smaller tests (to the left in the figure) suggest an approximately linear relationship, with a slope near unity, between reaction time at the confiner wall and acoustic transit time across the confiner wall. However, it appears that reaction time begins to level off at IDs ranging from 50.8 mm to 76.2 mm, where acoustic transit times are between 2.0 and 3.5 μs . For test 8-1855, with 76.2 mm ID, the acoustic transit times are around 3.25 μs and the estimated reaction time is close to that of test 8-1854, with a 50.8 mm ID. These results suggest that the maximum reaction zone timescale is approximately 2 μs for these experiments. Reactions are time-limited for the smaller tests by the thickness of the confiner wall, whereas high pressures are maintained for sufficiently long times in the larger tests for reactions to near completion.

6. Conclusions

Ammonal CYLEX tests conducted at scales ranging from 12.7 mm ID to 76.2 mm ID were examined using a newly developed low-pass filtering technique to process experimentally measured cylinder wall velocity profiles. This method better captured early motion of the confiner wall, and revealed an exper-

imental measurement of the shock-compression of the unreacted explosive along the Rayleigh line. However, the product isentrope computed from the filtered velocity profile was excessively noisy. Combining the low-pass filtering technique with the established method of fitting an equation to the experimental wall velocity data enabled construction of a composite isentrope. This composite isentrope captured compression along the Rayleigh line and a smooth isentropic expansion for all Ammonal CYLEX test scales considered.

Comparison of Ammonal performance across varying scales revealed highly non-ideal behavior. Detonation velocities decreased sharply with decreasing charge size, showing behavior much closer to ANFO than ideal explosives like PBX 9501. Wall expansion velocities increased with charge size, and maximum pressures computed from these velocity profiles increased significantly with scale for all diameters tested. JWL energy also increased dramatically with scale.

The empirical correlation model of Jackson [10] was applied to the Ammonal experiments using the parameters for aluminized explosives. Using only initial density and measured phase velocity with parameters calibrated with other tests, the model agreed remarkably well in terms of energy release and also predicted product isentropes well.

These results show that Ammonal is very sensitive to flow divergence behind the compression shock, and suggest a long reaction zone with a timescale on the order of $2 \mu\text{s}$. In a confined explosives test, high pressures behind the compression shock are maintained for times roughly equal to the acoustic transit time across the confiner wall. Plotting reaction time at the wall inferred from experimentally measured confiner velocity profiles versus the acoustic transit time revealed an approximately linear, one-one relationship at small scales, suggesting that reactions

are quenched before completion for these smaller tests. At larger scales, the reaction times leveled off, suggesting that reactions were no longer limited by time at high pressure behind the lead shock.

The strong variations in Ammonal performance as a function of scale present obvious modeling challenges. Over the range of scales considered here, it appears that scale-dependent product EOS and higher-order DSD relationships are needed to predict Ammonal behavior with programmed burn models.

Acknowledgements

Funding for this work was provided by the U.S. Department of Energy. The authors also thank Mark U. Anderson and Don W. Gilbert of Sandia National Laboratories for providing the Ammonal, and Bryce Tappan of Los Alamos National Laboratory for storing and blending the Ammonal.

References

- [1] S. I. Jackson, M. Short, Scaling of detonation velocity in cylinder and slab geometries for ideal, insensitive and non-ideal explosives, *J. Fluid Mech.* 773 (2015) 224–266.
- [2] S. I. Jackson, The dependence of ammonium-nitrate fuel-oil (anfo) detonation on confinement, *P. Combust. Inst.* 36 (2017) 2791–2798.
- [3] B. Zygmunt, Detonation parameters of mixtures containing ammonium nitrate and aluminium, *Cent. Eur. J. Energ. Mat.* 6 (2009) 57–66.

- [4] S. I. Jackson, An analytic method for two-dimensional wall motion and product isentrope from the detonation cylinder test, *P. Combust. Inst.* 35 (2015) 1997–2004.
- [5] P. Vitello, R. Garza, A. Hernandez, P. C. Souers, The energy diameter effect, *AIP Conf. Proc.* 955 (2007) 877–880.
- [6] D. L. Robbins, E. K. Anderson, M. U. Anderson, S. I. Jackson, M. Short, Cylinder test characterization of an ammonium nitrate and aluminum powder explosive, in: *Proceedings of the 15th International Symposium on Detonation*, Office of Naval Research, 2014, pp. 826–835.
- [7] E. K. Anderson, M. Short, S. I. Jackson, Cylinder test wall velocity profiles and product energy for an ammonium nitrate and aluminum explosive, *AIP Conf. Proc.* 1793 (2017) 030018–1–030018–5.
- [8] M. A. Cook, A. S. Filler, R. T. Keys, W. S. Partridge, W. O. Ursenbach, Aluminized explosives, *J. Phys. Chem.-US* 61 (1957) 189–196.
- [9] O. T. Strand, D. R. Goosman, C. Martinez, T. L. Whitworth, W. W. Kuhlow, Compact system for high-speed velocimetry using heterodyne technique, *Rev. Sci. Instrum.* 77 (8) (2006) 083108.
- [10] S. I. Jackson, Scaling of the detonation product state with reactant kinetic energy, *Combust. Flame* 190 (2018) 240–251.
- [11] P. C. Souers, L. Lauderbach, R. Garza, L. Ferranti, P. Vitello, Upgraded analytical model of the cylinder test, *Propell. Explos. Pyrot.* 38 (2013) 419–424.

- [12] L. Hill, Detonation product equation of state directly from the cylinder test, *Int. Symp. Shock Waves* 955 (1997) 355–360.
- [13] E. Lee, H. Hornig, Equation of state of detonation product gases, *Symp. (Int.) Combust.* 12 (1) (1969) 493 – 499.
- [14] W. A. Trzcíński, S. Cudziło, J. Paszula, J. Callaway, Study of the effect of additive particle size on non-ideal explosive performance, *Propell. Explos. Pyrot.* 33 (2008) 227–235.
- [15] V. J. Bellitto, M. I. Melnik, M. H. Sherlock, J. C. Chang, J. H. O'Connor, J. A. Mackey, Microstructure effects on the detonation velocity of a heterogeneous high-explosive, *J. Energ. Mater.* 36 (4) (2018) 485–492.

List of Figures

1	Diameter-effect curves for ideal and non-ideal explosives, adapted from [1].	18
2	Three in. ID Ammonal CYLEX test. The streak camera window is shown on the left and an image of the experiment is shown on the right.	19
3	Velocity profiles for the 50.4 mm ID test, 8-1854, top, and the 76.2 mm ID test, 8-1855, bottom. The color of each velocity profile corresponds to the axial position of the probe according to the plot legends. Axial probe positions are provided as percentage of run distance, where 0 % is the initiation plane and 100 % is the end of the test. In cases where multiple measurements were made at the same axial position, averaged velocity profiles are shown. A zoomed view in the lower right of each plot shows the profiles late in the expansion.	20
4	Experimentally measured CYLEX velocity profile (blue), fit to Eq. 1 (orange), and low-pass filtered profile (red). Profiles are for 8-1855 (76.2 mm ID), probe 7 (37% of run distance). The inset shows a zoomed view of the early confiner motion.	21
5	Isentropes computed from a low-pass filtered velocity profile (green) and a fitted velocity profile (blue) for 8-1855 (76.2 mm ID) CYLEX test, probe 7 (37% of run distance). The theoretical Rayleigh line is shown in black. The blue circle shows maximum pressure on the isentrope while the red circle shows 0.5 % divergence between the experimental Rayleigh line and fitted isentrope.	22
6	Composite isentropes for scaled Ammonal CYLEX tests. Test inner diameters are labeled in figure. Isentropes for the 12.7 mm and 25.4 mm tests were generated for the tests reported in [5]. The blue circles show maximum pressure on the isentropes while the red circles show 0.5 % divergence between the experimental Rayleigh line and fitted isentrope for each case.	23
7	Isentropes for 8-1854 (top) and 8-1855 (bottom) computed directly from experimental data (black points). Both figures show isentropes for probes located at 68% of run distance. Also shown are the Rayleigh lines (pink), JWL fits of Table 2 (red), and the isentrope predicted by the empirical correlation model (blue).	24

8 JWL energy as a function of reactant kinetic energy. The red and blue circles represent energies computed from experimental results, while the open circles represent the energy computed using the empirical correlation model [10] for the initial density and measured phase velocity of each test. The e_0 values shown are the average of the values measured at 68% run distance for the LANL tests. The line shows e_0 predicted by the model assuming initial density equal to the average of the six experiments. 25

9 Reaction time at the confiner wall plotted as a function of acoustic transit time across the confiner wall. LLNL tests are shown with red markers while 8-1854 and 8-1855 are shown with blue markers. The line represents values with reaction times equal to the acoustic transit time. 26

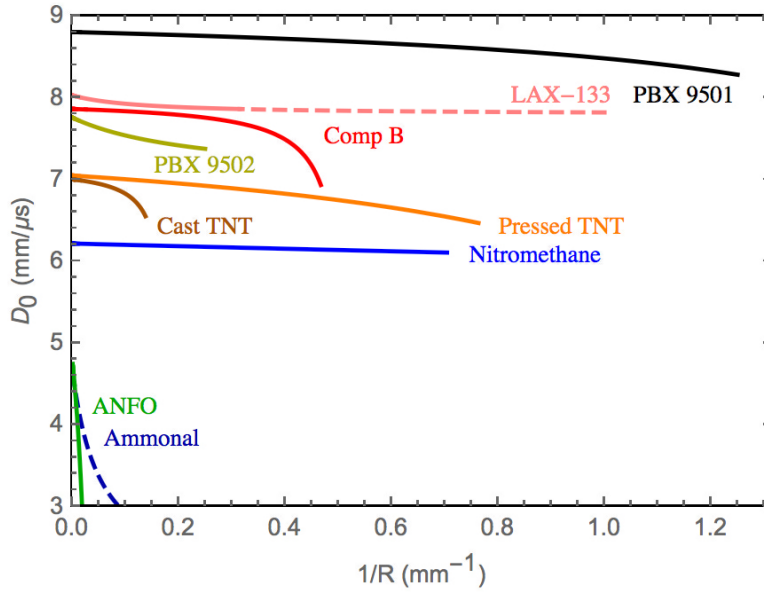


Figure 1: Diameter-effect curves for ideal and non-ideal explosives, adapted from [1].

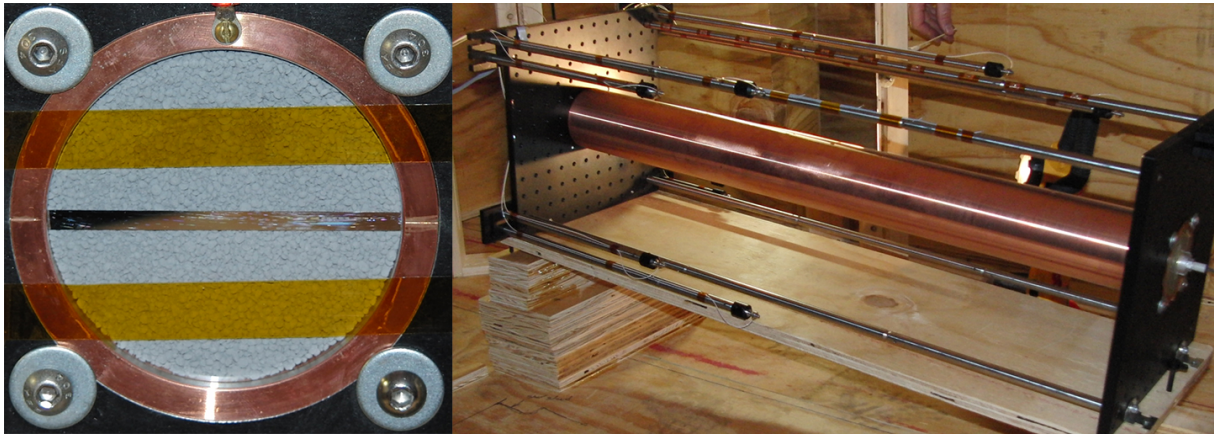


Figure 2: Three in. ID Ammonal CYLEX test. The streak camera window is shown on the left and an image of the experiment is shown on the right.

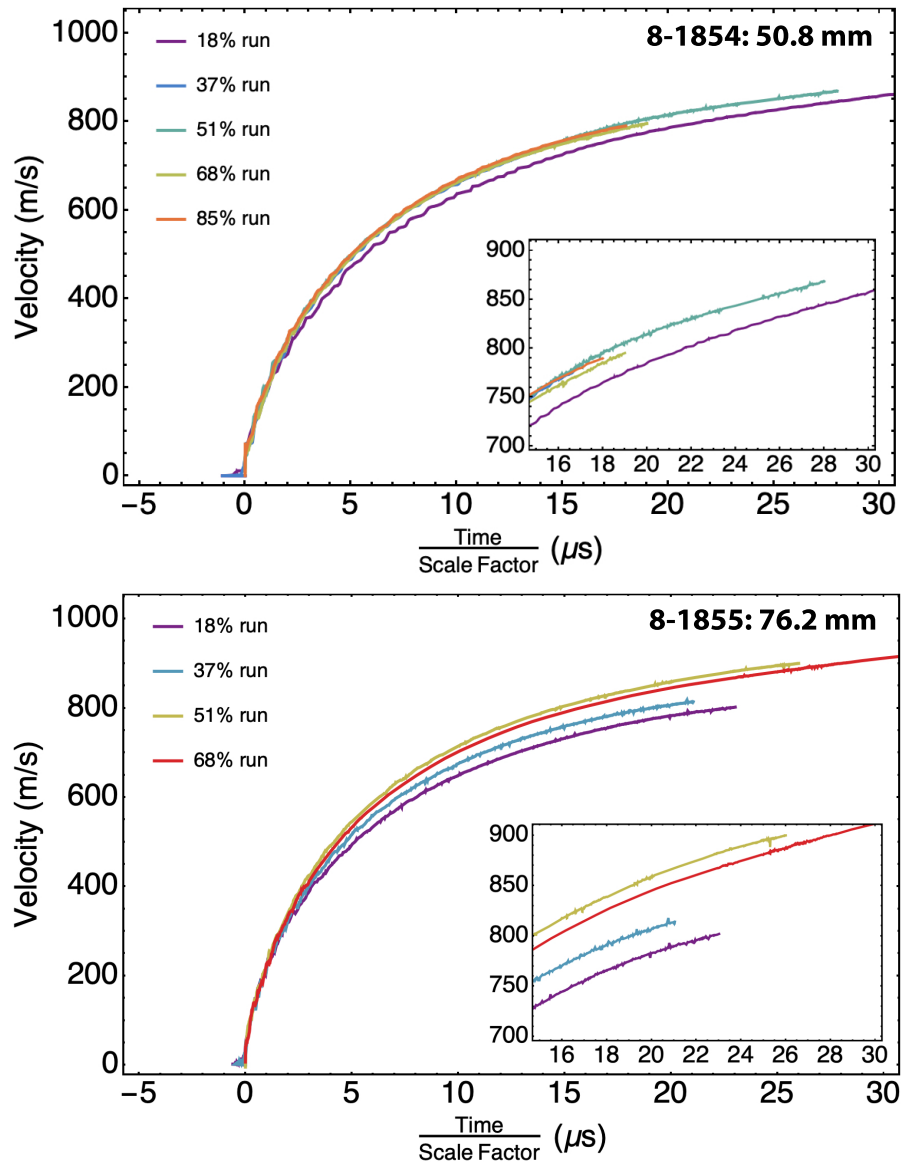


Figure 3: Velocity profiles for the 50.4 mm ID test, 8-1854, top, and the 76.2 mm ID test, 8-1855, bottom. The color of each velocity profile corresponds to the axial position of the probe according to the plot legends. Axial probe positions are provided as percentage of run distance, where 0 % is the initiation plane and 100 % is the end of the test. In cases where multiple measurements were made at the same axial position, averaged velocity profiles are shown. A zoomed view in the lower right of each plot shows the profiles late in the expansion.

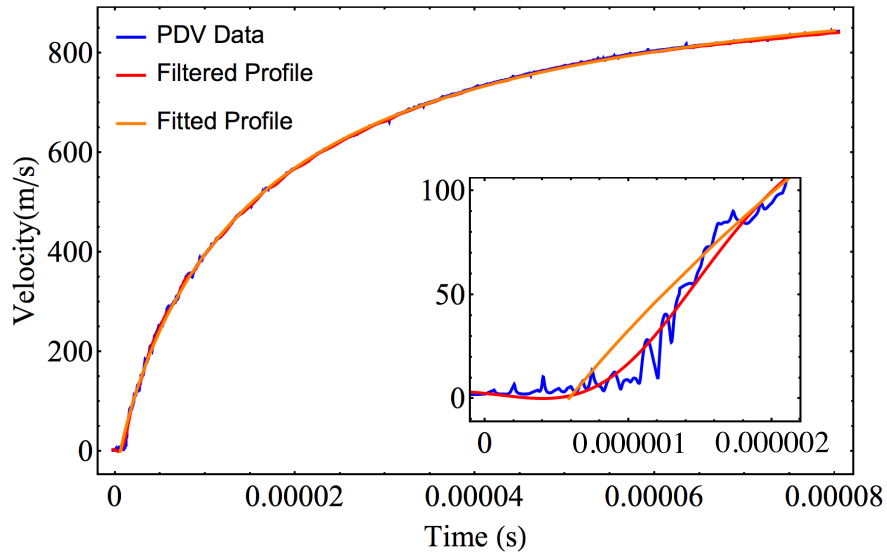


Figure 4: Experimentally measured CYLEX velocity profile (blue), fit to Eq. 1 (orange), and low-pass filtered profile (red). Profiles are for 8-1855 (76.2 mm ID), probe 7 (37% of run distance). The inset shows a zoomed view of the early confiner motion.

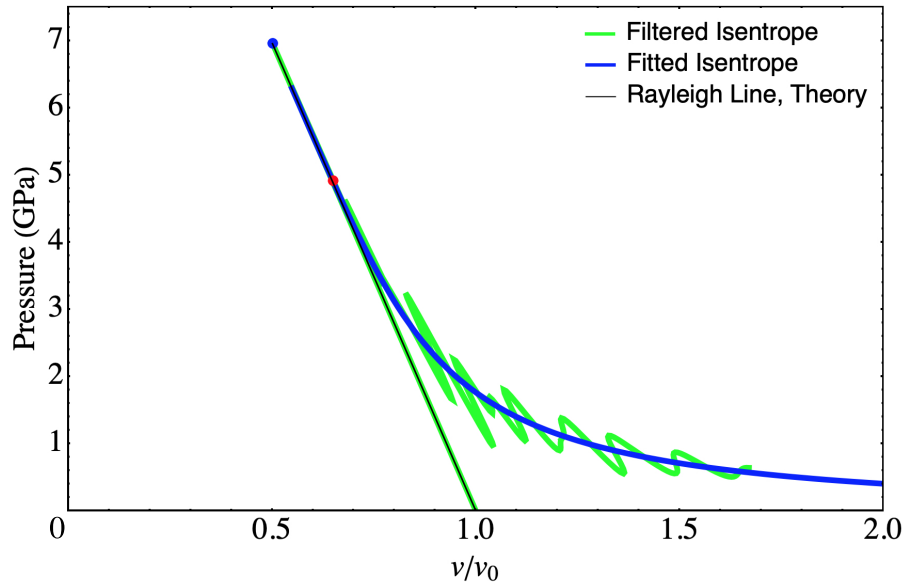


Figure 5: Isentropes computed from a low-pass filtered velocity profile (green) and a fitted velocity profile (blue) for 8-1855 (76.2 mm ID) CYLEX test, probe 7 (37% of run distance). The theoretical Rayleigh line is shown in black. The blue circle shows maximum pressure on the isentrope while the red circle shows 0.5 % divergence between the experimental Rayleigh line and fitted isentrope.

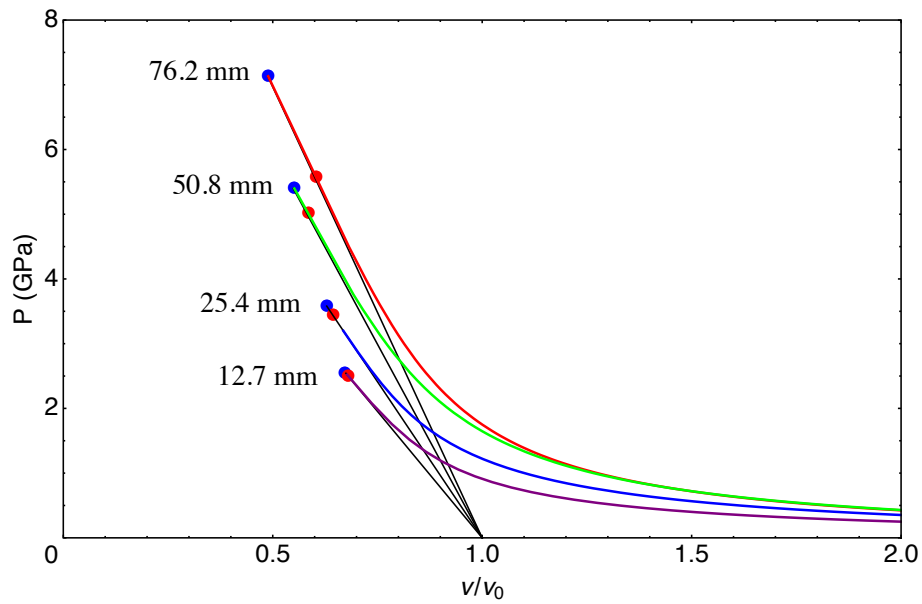


Figure 6: Composite isentropes for scaled Ammonal CYLEX tests. Test inner diameters are labeled in figure. Isentropes for the 12.7 mm and 25.4 mm tests were generated for the tests reported in [5]. The blue circles show maximum pressure on the isentropes while the red circles show 0.5 % divergence between the experimental Rayleigh line and fitted isentrope for each case.

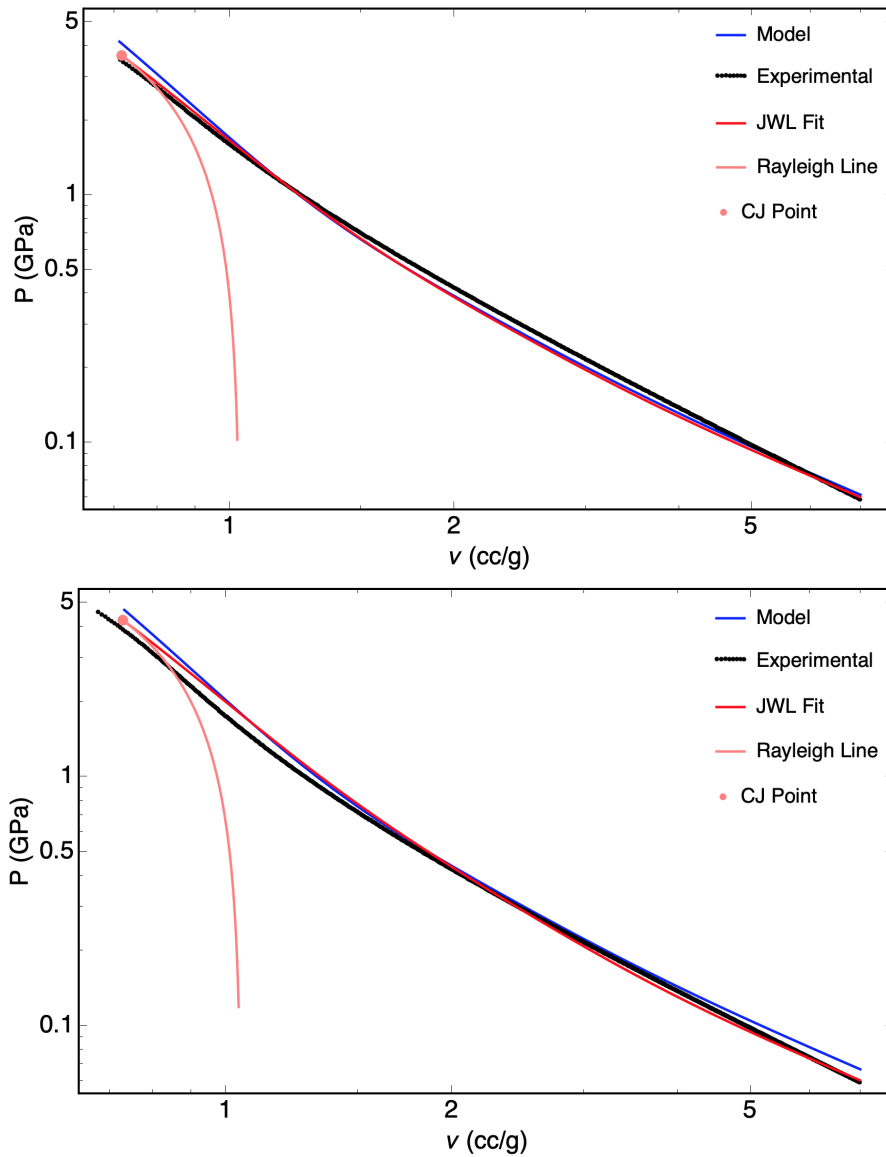


Figure 7: Isentropes for 8-1854 (top) and 8-1855 (bottom) computed directly from experimental data (black points). Both figures show isentropes for probes located at 68% of run distance. Also shown are the Rayleigh lines (pink), JWL fits of Table 2 (red), and the isentrope predicted by the empirical correlation model (blue).

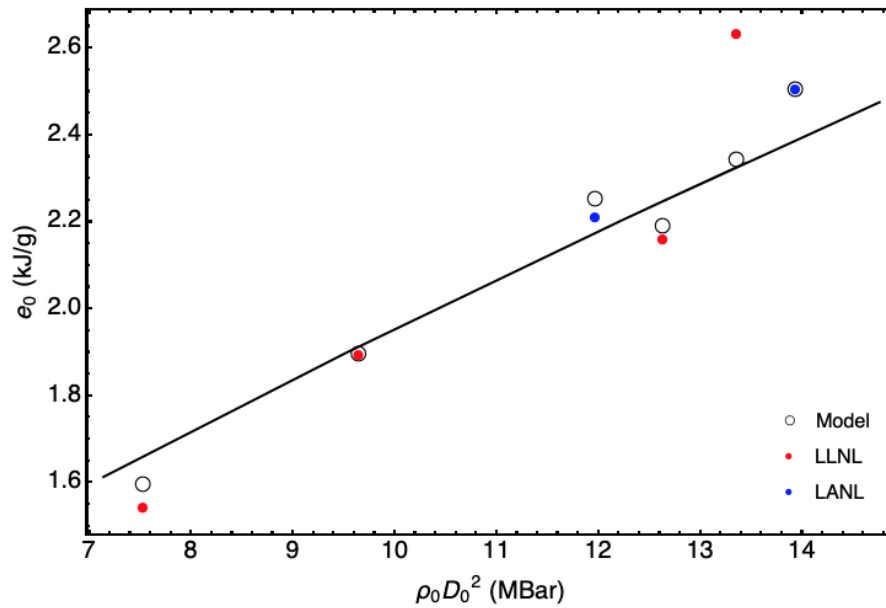


Figure 8: JWL energy as a function of reactant kinetic energy. The red and blue circles represent energies computed from experimental results, while the open circles represent the energy computed using the empirical correlation model [10] for the initial density and measured phase velocity of each test. The e_0 values shown are the average of the values measured at 68% run distance for the LANL tests. The line shows e_0 predicted by the model assuming initial density equal to the average of the six experiments.

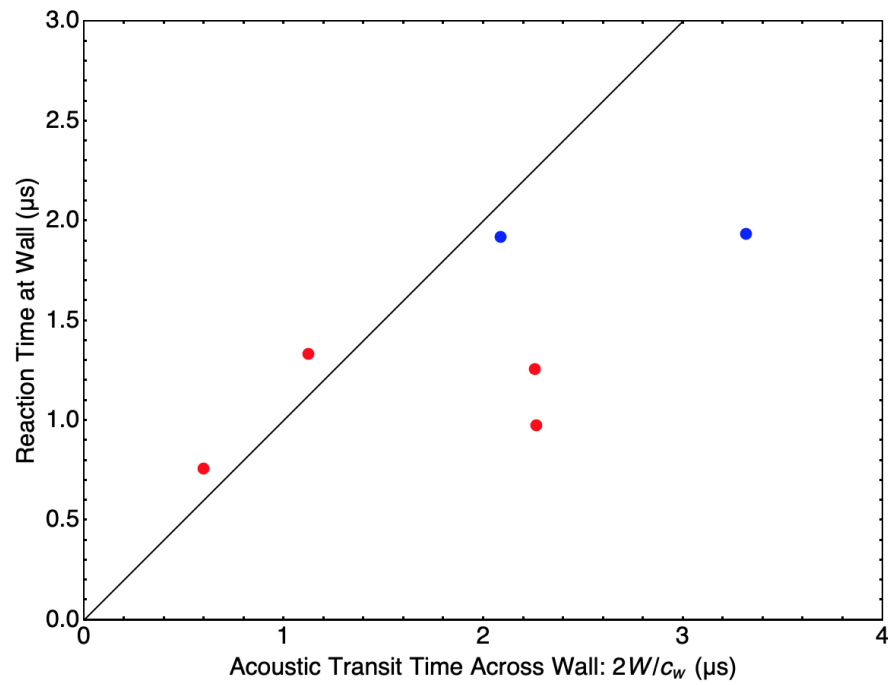


Figure 9: Reaction time at the confiner wall plotted as a function of acoustic transit time across the confiner wall. LLNL tests are shown with red markers while 8-1854 and 8-1855 are shown with blue markers. The line represents values with reaction times equal to the acoustic transit time.

List of Tables

1 Experimental specifics of Ammonal CYLEX tests. All tests were conducted using blends of 90% AN and 10% Al powder by mass. Tests marked LLNL were reported by Vitello et al. [5]. The LLNL test numbers correspond to the order in which they appear in Table 1 of [5]. Note that the test designated LLNL 4 is listed twice in [5], presumably because there were two PDV probes on the same test. 28

2 JWL fit parameters for each probe measuring wall velocity for the tests listed in Table 1. The LLNL tests were fielded with PDV probes angled 7° toward the initiation plane of the experiments [5]. A correction was applied to compute the parameters shown. . . 29

Table 1: Experimental specifics of Ammonal CYLEX tests. All tests were conducted using blends of 90% AN and 10% Al powder by mass. Tests marked LLNL were reported by Vitello et al. [5]. The LLNL test numbers correspond to the order in which they appear in Table 1 of [5]. Note that the test designated LLNL 4 is listed twice in [5], presumably because there were two PDV probes on the same test.

Test #	Confiner ID (mm)	Confiner OD (mm)	Ammonal Initial Density (g/cc)	Al Particle Diameter (μm)	D_0 (mm/ μs)
8-1855	76.20	91.44	0.953	2.05	3.824 \pm 0.009
8-1854	50.80	60.96	0.968	2.05	3.516 \pm 0.020
LLNL 1	50.82	61.24	1.044	5	3.673
LLNL 2	50.86	61.24	1.002	95	3.486
LLNL 3	25.44	30.60	1.023	20	3.068
LLNL 4	12.70	15.42	1.023	20	2.644

Table 2: JWL fit parameters for each probe measuring wall velocity for the tests listed in Table 1. The LLNL tests were fielded with PDV probes angled 7° toward the initiation plane of the experiments [5]. A correction was applied to compute the parameters shown.

Test #	Probe Position (% run distance)	A (GPa)	B (GPa)	C (GPa)	R_1	R_2	ω	v_{CJ} (cc/g)	P_{CJ} (GPa)	e_0 (kJ/g)
LLNL 1	N/A	44.2	2.99	0.797	4.5	1.5	0.28	0.642	4.590	2.629
LLNL 2	N/A	45.2	1.83	0.674	4.5	1.5	0.28	0.688	3.766	2.156
LLNL 3	N/A	32.8	1.19	0.685	4.5	1.5	0.28	0.665	3.082	1.889
LLNL 4 P1	N/A	24.9	0.645	0.0.645	4.5	1.5	0.28	0.640	2.395	1.539
LLNL 4 P2	N/A	27.0	0.622	0.622	4.5	1.5	0.28	0.651	2.309	1.488
8-1854	84.6	44.0	2.31	0.570	4.5	1.5	0.28	0.709	3.748	2.143
8-1854	84.6	41.1	2.78	0.549	4.5	1.5	0.28	0.700	3.854	2.223
8-1854	68	44.7	1.91	0.639	4.5	1.5	0.28	0.712	3.715	2.243
8-1854	68	46.3	1.48	0.691	4.5	1.5	0.28	0.717	3.658	2.172
8-1854	51	42.5	2.00	0.681	4.5	1.5	0.28	0.706	3.783	2.280
8-1854	51	43.9	1.77	0.693	4.5	1.5	0.28	0.711	3.735	2.246
8-1854	37	45.6	1.37	0.733	4.5	1.5	0.28	0.716	3.673	2.224
8-1854	18	48.2	1.28	0.681	4.5	1.5	0.28	0.723	3.597	2.105
8-1855	68	54.7	2.18	0.682	4.5	1.5	0.28	0.729	4.250	2.443
8-1855	68	51.8	2.38	0.715	4.5	1.5	0.28	0.723	4.339	2.559
8-1855	51	55.9	2.12	0.660	4.5	1.5	0.28	0.732	4.214	2.575
8-1855	51	45.0	3.61	0.643	4.5	1.5	0.28	0.703	4.594	2.734
8-1855	37	56.0	2.69	0.532	4.5	1.5	0.28	0.731	4.229	2.281
8-1855	18	61.8	2.02	0.526	4.5	1.5	0.28	0.744	4.049	2.105